# Numerical Investigation for Heat Transfer Enhancement Using Nanofluids Over Ribbed Confined One-End Closed Flat-Plate

Mohamed M. Hassan [a], Mohamed A. Teamah [b], Wael M. El-Maghlany [c]

[a] Facultyof Engineering, Pharos University,Egypt
[b] Arab Academyfor Scienceand Technologyand Maritime Transport,Egypt
[b, c] Facultyof Engineering,Alexandria University,Egypt

**Abstract**—Jet impingement is one of various methods of cooling with the ability to achieve high heat transfer rates and improve average surface's Nusselt number. This method has vast industrial applications including: integrated use in solar collectors, gas turbine cooling, refrigeration, air conditioning and electronics cooling. A numerical study is conducted to study the effect of using nanofluids on impinging slot jet over a flat plate with a ribbed surface. The main objective of the study is to investigate the possibility of improving the overall heat transfer rate by focusing on the improvements in the local and average surface Nusselt number values. Several parameters effects are studied including, Solid Volume Fraction, Richardson number, Reynolds number. The results indicated a marked improvement in average Nusselt number with the increase in the solid volume fraction and amended values when buoyancy effect is dominant over the whole domain. The results are summarized in form of streamlines, isotherms and Nusselt number contra other variables. The current work was simulated using a FORTRAN CFD Code, which discretize the non-dimensional forms of the governing equations utilizing the finite volume method and solve the consequent algebraic equations using Gauss-Seidal method Utilizing TDMA.

**Index Terms**—Heat Transfer, Impinging Jet, Slot Jet, Mixed convection, Rib, Laminar.



## 1 INTRODUCTION

Nanofluids has been one of the interests of researchers to enhance heat transfer rates in industrial thermal systems. Where base fluids are known for having low thermal conductivity, so the need to improve the thermal conductivity lead to the use of nanoparticles in base fluid to improve the effective thermal conductivity and other fluid thermal properties.there are two categories of Nanofluids metallic and non-metallic based on the type of nanoparticles used such as $\mathbf{Al_2O_3}, \mathbf{Ag}, \mathbf{CuO}, \mathbf{Cu}, \mathbf{SiO_2}$ and $\mathbf{TiO_2}$[1].Various heat transfer enhancement techniques were researched to increase local heat transfer coefficient ,however, a method emerged where a jet is directed to impinge on a heated surface with the goal to cool it and with the capacity to deal with high heat flux .Jet Impingement has proven to be one of the eminent methods for enhancing heat transfer but dealing with the low thermal properties of the normal working fluids either air or water lead to a less expected results so a mixture of nanoparticles with one of those base fluids is expected to give a higher heat transfer rates [2]. Jet Impingement using Nanofluids have been studied extensively numerically and experimentally where Li et al. 2011 [3] investigated both jet impingement and forced convection,where he concentrated on the performance of N in submerged configuration.The results presented showed that improvements in the heat transfer compared to pure water and presented correlations with agreement of experimental results for calculation of Nusselt Number at given solid volume fraction , jet to plate spacing and Reynolds number.El-Maghlany et al. 2015 [4] numerically investigated the effect of Nanofluids on the thermal performance of ribbed flat plate using Cu-Water Nanofluids. Teamah et al. 2016 [5] numerically and experimentally investigated flow structure and heat transfer of jet cooling over flat plat utilizing Nanofluids ($\mathbf{Al_2O_3}$),the mathematical model was derived and numerically solved using Finite volume with SIMPLER algorithm. Manca et al. 2016 [6] numerically investigated confined slot jet using Nanofluids and pure water for laminar steady state conditions, comparison for various Reynolds Number, Solid Volume Fraction and Plate to jet spacing ratio were provided. Heshmati et al. 2014 [7] investigated mixed convection heat transfer characteristics numerically for the effect of Nanofluids on a two dimensional backward facing step .the governing equations were solved using FVM with SIMPLE algorithm to link velocity and pressure fields for different Reynolds number. Dutta et al. 2016 [8]numerically investigated the behavior of hydrodynamic and heat transfer for $\mathbf{Al_2O_3 - Water}$ Nanofluids for both laminar and turbulent confined slot jet where he studied the effect of solid volume fraction at 3 and 6% using a single phase fluid approach to model the Nanofluids. Nguyen et al. 2008 [9] experimentally investigated effect of temperature and solid volume fraction on dynamic viscosity for two different nanoparticle size where the data were collected from commercial viscometer piston type at room conditions up to $\mathbf{75}$ ℃ .Huang et al. 2013 [10] numerically investigated effect of $\mathbf{Al_2O_3 - Water}$ Nanofluids on confined circular jet impinging for turbulent flow over a

flat plate at constant wall temperature for different jet to plate spacing ratio, solid volume fraction and Reynolds number where he observed that a maximum of 10% is obtained when compared to performance using pure water at jet to plate spacing of 5.Singh et al. 2016 [11] experimentally investigated the effect of laminar Nanofluid jet on a heated steel surface and compared it with water jet. The effect of concentration and jet velocity for $\mathbf{TiO_2}$based Nanofluid was evaluated experimentally and the results showed an enhancement compared to water results , furthermore an increase in the concentrated leads to increase in the average heat transfer rate.Maïga et al. 2005 [12] investigated the hydrodynamic and thermal characteristics of laminar forced convection flow of Nanofluid on two geometries using numerical simulation. Where results clearly revealed that addition of nanoparticles have increase the heat transfer when compared to base fluid.Dagtekin et al. 2008 [13] investigated the heat transfer due to double impinging vertical slot jet on an isothermal wall for laminar flow using Finite Volume Method on a non-staggered grid arrangement using SIMPLEM to study the effect of Reynolds number, jet to plate spacing, jet to jet spacing on the heat transfer and flow field.

## 2 Mathematical Formulation

### 2.1 Dimensional Model and Governing Equations

A two-dimensional Confined Slot Jet laminar mixed convection flow over ribs on a flat plate is numerically investigated utilizing Cu-Water as the working. The Dimensional model with computational domain is shown in Fig.1, Where the upper plate is confined and contain a single slot jet inlet port, the lower plate is isothermal, both the left-hand side end and the upper plate are adiabatic and the right-hand side end is open to allow the flow to escape. The model is solved with reference to the jet width so some parameters are introduced at first then a dimensionless parameter are constructed to solve the problem. The plate length is long enough to satisfy the fully developed laminar flow exit condition (L = 20W).the variable parameters that are changed during the problem solving are as follows $b/W = 3,4,5$ ,$H/W = 12,15,18,21$,$a/b = 1,1.5,2$ respectively, The Reynolds number $50 < Re < 350$ ,Richardson Number $0.1 < Ri < 1$ are changed to study their effect on the fluid flow field and the heat transfer characteristics. The objective of the present work is to study the effect of the changed parameters on Nusselt Number of the Nanofluid when compared to that of Pure water for different Solid Volume Fraction.it should be noted that some assumptions are made to simplify the analysis which are the flow is steady state, two-dimensional, laminar, Newtonian ,Incompressible, Radiation is neglected along the walls, thermal properties of Nanofluid are constant except density which is acted upon by the buoyancy force only determined by the Boussinesq approximation, the nanoparticles and water are in thermal equilibrium and no-slip condition occurs.The thermal properties of the Nanofluid which is a mixture of water and Cu nanoparticles can be calculated by a set of equations with solid volume fraction as the main variable parameter:

The Effective density of the Nanofluid can be calculated using Vajjha 2009 [14] :

$$\rho_{eff} = (1-\phi)\rho_{bf} + \phi\rho_p \quad (1)$$

Where $\rho_{bf}$ and $\rho_p$ are the densities of the base fluid and solid nanoparticles ,respectively.

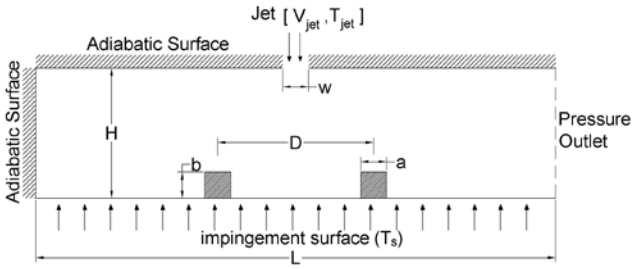


Fig. 1. Schematic Diagram of Two-Dimensional Slot-Jet Configuration

The Effective heat capacity at constant pressure can be calculated using Vajjha 2009 [14] :

$$(\rho C_p)_{eff} = (1-\phi)(\rho C_p)_{bf} + \phi(\rho C_p)_p \quad (2)$$

Where $(\rho C_p)_{bf}$and $(\rho C_p)_p$ are heat capacities of base fluid and nanoparticles ,respectively.

The Thermal expansion coefficient was suggested by Hwang 2007 [15] as follows :

$$\beta_{eff} = (1-\phi)\beta_{bf} + \phi\beta_p \quad (3)$$

Where $\beta_{bf}$and $\beta_p$ are thermal expansion coefficient of base fluid and nanoparticles ,respectively.

The Thermal conductivity for liquid-solid mixture depending on nanoparticles concentration and particle dimensions varying from $10^{-6}$ to $10^{-3}$ m for very low volume fractions was proposed by Maxwell 1873 [16] as follows :

$$\frac{k_{eff}}{k_{bf}} = \frac{k_p + 2k_{bf} + 2\phi_p(k_p - k_{bf})}{k_p + 2k_{bf} - \phi_p(k_p - k_{bf})} \quad (4)$$

The effective viscosity of was related to be dependent on viscosity of base fluid depending upon the volume fraction percentage by weight , where Einstein 1906 [17] expressed the effective viscosity of spherical solids as a function of volume fraction for low levels of concentration as follows :

$$\mu_{eff} = (1 + 2.5\phi)\mu_{bf} \quad (5)$$

The thermal properties of the Nanofluid used and water can be tabulated as shown below in Table 1.

**TABLE 1**
THERMAL PROPERTIES FOR PURE WATER AND CUO NANOFLUID AT

| Thermal Properties | Water | Cu | | |
|---|---|---|---|---|
| $\rho\,(kg/m^3)$ | 996.5 | 6500 | | |
| $C_p(J/kg.K)$ | 4182.2 | 535.6 | | |
| $k\,(W/m.K)$ | 0.613 | 20 | | |
| $\mu\,(N.s/m^2)$ | $2.01E-3$ | - | | |
| $\beta\,(K^{-1})$ | $21.0E-5$ | *Temperature* | *Concentration (%)* | *Value* |
| | | $298\,K \le T \le 363\,K$ | $1 \le \phi \le 6$ | $9.881(100\phi)^{-0.9446}$ |

$T = 300\,K$ MOHAMMED 2012 [18]

The following dimensionless parameters are introduced:

$$X = \frac{x}{w}, \quad Y = \frac{y}{w}, \quad U = \frac{u}{V_j}, \quad V = \frac{v}{V_j}, \quad \theta = \frac{T_i - T_j}{T_s - T_j}$$

$$Re = \frac{\rho w V_j}{\mu}, \quad Gr = \frac{g\beta w^3 (T_s - T_j)}{\nu^2}, \quad Ri = \frac{Gr}{\mathrm{Re}^2}, \quad \alpha = \frac{k}{\rho C_p}, \quad \mathrm{Pr} = \frac{\nu_{bf}}{\alpha_{bf}}$$

The continuity, momentum and energy governing equations in the non-dimensional Cartesian coordinates form are given as follows:

$$\frac{\partial U}{\partial X} + \frac{\partial V}{\partial Y} = 0 \tag{6}$$

$$\left[U\frac{\partial U}{\partial X} + V\frac{\partial U}{\partial Y}\right] = -\frac{\partial P}{\partial X} + \frac{\mu_{nf}\rho}{\mu\rho_{nf}}\frac{\lambda}{Re}\left[\frac{\partial^2 U}{\partial X} + \frac{\partial^2 U}{\partial Y}\right] \tag{7}$$

$$\left[U\frac{\partial V}{\partial X} + V\frac{\partial V}{\partial Y}\right] = -\frac{\partial P}{\partial Y} + \frac{\mu_{nf}\rho}{\mu\rho_{nf}}\frac{\lambda}{Re}\left[\frac{\partial^2 V}{\partial X} + \frac{\partial^2 V}{\partial Y}\right] + \frac{\beta_{nf}}{\beta} Ri\,\theta \tag{8}$$

$$\left[U\frac{\partial \theta}{\partial X} + V\frac{\partial \theta}{\partial Y}\right] = \frac{\alpha_{nf}}{\alpha}\frac{\Omega}{Re\,Pr}\left[\frac{\partial^2 \theta}{\partial X^2} + \frac{\partial^2 \theta}{\partial Y^2}\right] \tag{9}$$

Where in Solid Domain,

$$\lambda = \infty, \quad \Omega = \frac{k_{fin}}{k_{fluid}}$$

And in Fluid Domain,

$$\lambda = 1, \quad \Omega = 1$$

The Assigned boundary conditions for the non-dimensional equations 6 → 9 are given as follows :

- The top wall is adiabatic where at the jet exit $U = 0, V = -1, \theta = 0$ and at the adiabatic surface $U = 0, V = 0, \frac{\partial \theta}{\partial Y} = 0$.
- The bottom wall is isothermal where $U = 0, V = 0, \theta = 1$.
- The left wall is adiabatic where $U = 0, V = 0, \frac{\partial \theta}{\partial X} = 0$.
- The right hand side is open end for flow to escape $\frac{\partial U}{\partial X} = 0, V = 0, \frac{\partial \theta}{\partial X} = 0$.

### 2.2 Nusselt Number

The local Nusselt Number the surface of the bottom isothermal plate is given by:

$$Nu = \frac{hw}{k} = \frac{q_s w}{k_{eff}\left(T_s - T_j\right)} \tag{10}$$

In addition, the average Nusselt Number for the lower isothermal plate can be calculated by:

$$\overline{Nu}_{(w)} = \frac{1}{A_1 + 2A_2 + 4A_3}\int_0^{(A_1+2A_2+4A_3)} Nu_{(w)}\,dN \tag{11}$$

Where the bottom plate areas (Shown in Fig.2) can be calculated as follows:

$$A_1 = \frac{X_1 + X_2 + X_3}{w} = \frac{L - 2a}{w} \tag{12}$$

$$A_2 = \frac{a}{w} \tag{13}$$

$$A_3 = \frac{b}{w} \tag{14}$$

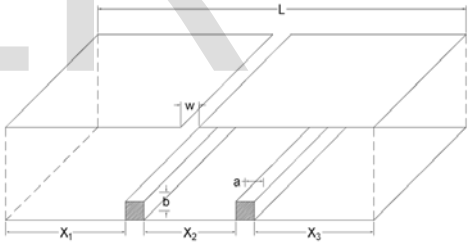


Fig. 2. Bottom's Plate Nusselt number area.

### 2.3 Grid Independency and Code Validation

The Grid independency was check to obtain the optimum computation grid and find the effect of changing the grid system size on the results, where six different grid systems were check $(100 \times 20, 200 \times 40, 300 \times 60, 400 \times 80, 500 \times 100, 900 \times 180)$ were investigated for $\mathrm{Re} = 100, \phi = 3\%, \mathrm{Ri} = 1, \mathrm{b/w} = 3$.Where the results Shown in Table 2 shows a small error of almost 4% as it clearly shown in Fig.3 and Fig.4 ,so to obtain the appropriate results at an less time a domain grid of $300 \times 60$ was adopted. The code validation was done based on boundary conditions and configuration reported by Manca and D.Ricci 2011 [19].The research work was focused on numerical simulated of laminar mixed convection single slot jet with both sides open for flow escape utilizing $Al_2O_3$ Nanofluid for variable solid-volume fraction. The comparison of the present study and the results presented by Manca and D.Ricci

2011[19] shows clearly a good agreement as shown in Fig.5 and streamlines shown in Fig.6.

**TABLE 2**

| Grid System | $Nu_{avg}$ |
|---|---|
| 100x20 | 14.62 |
| 200x40 | 7.423 |
| 300x60 | 2.129 |

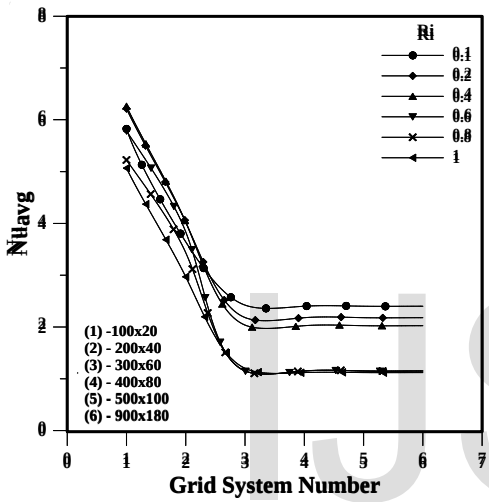


Fig. 3. Grid Independency at Constant Ri Number for Various Grid Systems.

| | |
|---|---|
| 400x80 | 2.024 |
| 500x100 | 2.018 |
| 900x180 | 2.012 |

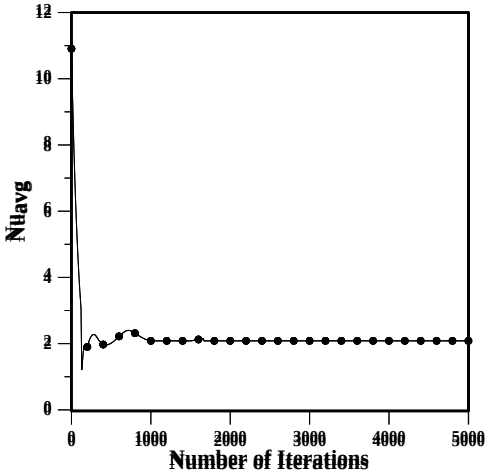


Fig. 4. Stability of Nusselt number for various number of iterations.

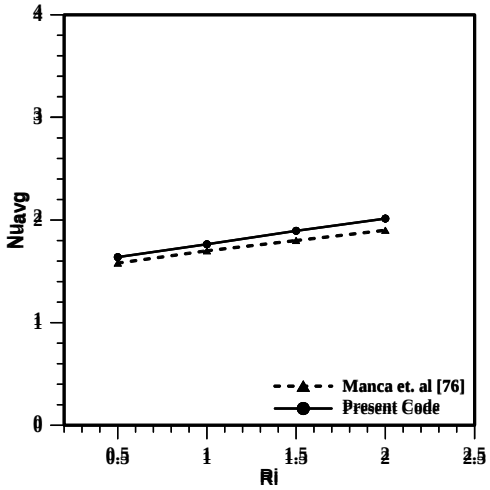


Fig. 5. Comparison between current code and results presented by Manca and D.Ricci 2011[19]

### 2.4 Solution Procedures

The current work code is Fortran code based on Finite-Volume Method (FVM) for numerical simulation and discretization of incompressible Non-Dimensional Navier-Stokes Equations, where pressure and velocity field are linked which was conducted by SIMPLE Algorithm utilizing TDMA introduced by Patankar 1980 [20] .The convergence of the iteration is determined by change in the average Nusselt Number as well as other dependent variables through one hundred iterations to be less than 0.01% of its initial value

## 3 Results and Discussion

Prior to the validation of the Fortran code and Confirming the

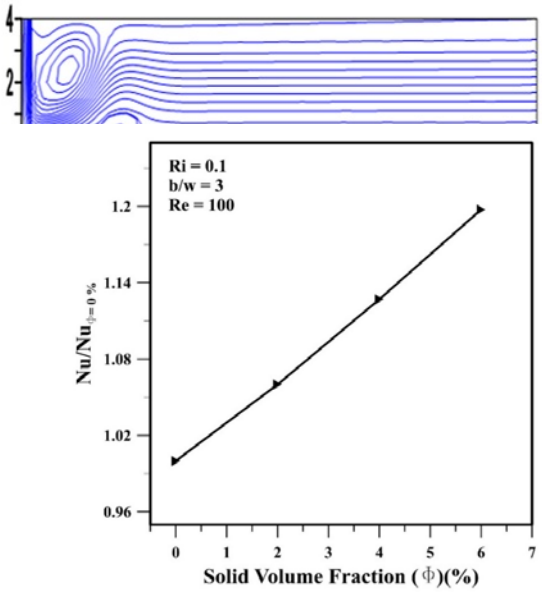


Fig. 7. Effect of Solid Volume Fraction on Average Nusselt number.

grid independence, the results will be shown in the following sections. The computational domain is positioned showing the inlet and outlet of the configuration with one side closed but in some cases in order to display the effects clearly only regions near the ribs are shown. The presented results for the convective jet cooling on a flat plate with two mounted ribs upon an isothermal wall are presented. The effects Re,Ri($Gr/(Re^2$ )),φ on the flow and heat transfer are numerically examined.CuO-Water Nanofluids is considered as the working fluid. In this regard, Prandtl number is taken as 6.2 through this study. The ribs are positioned from the left corner at X=5,14 respectively .For comparison purposes , RI is kept constant at 0.1 , Re is kept constant at 141,the rib height to jet width ratio is 3.For illustrating the results the particle volume fraction φ is set equal to 0,2%,4%,6% by wt. .the results of this section illustrated using the streamlines and temperature field through the whole computational domain are presented.Futher results may include changing in Richardson ,Reynolds ,ribs position and rib height to width ratio to indicate the effect of these parameters of the flow and heat transfer.

### 3.1 Effect of Particle Volume Fraction

The effect of nanoparticle concentrations on Nusselt number is shown in Figure 6. The data indicates that, for constant Reynolds number, the Nusselt number increases as the nanoparticle concentration increases. The highest values of Nusselt number are gained at higher level of concentration of solid nanoparticles which is related to the increasing profile in the buoyancy effect, However, the data in Figure 6 shows that for 2,4 and 6% nanoparticle concentration an increase in Nusselt number can be shown in terms of pure water respectively 7,13,20 %. Figure 7, shows another representation of the data where the stream lines are shown for pure water and three concentrations of nanoparticles 2,4 and 6%. Although, flow feature of viscosity is a crucial point for heat transfer improvement thus using nanofluids or increasing its concentration doesn't mean an imminent increase in the heat transfer rate, rather than the fact that the viscosity increase sharply when increase the concentration of nanoparticles dispersed in the base fluid and transcend that of base fluid, so that the flow rate reaching the contact surface is miniscule. Figure 6 and 7 illustrates the plot of stream function and isotherms at various nanoparticle concentrations for Re = 141, RI = 0.1. The effect of natural convection is rather clear where small eddy is observed at the leading edge of the rib, whereas the concentration of nanoparticles decreases the eddies becomes even smaller where the recirculation region at the trailing edge of the ribs enlarge. The overseen characteristic of flow is expected due to the keen buoyant up flow which inhibits recirculating eddy, although, the strength of the vortex increases as the concentration of nanoparticles progresses the streamlines begin to skew to the right direction due to the positive pressure being exerted on the fluids starting from the separation location farther from the stagnation point till it re-converge again downstream from the trailing edge of the fin ,thus an accretion in the shear stress between the layers of fluid flow is observed. Furthermore, as recirculation regions correlates to an area with low heat transfer rate. It can be observed that the reattachment length changes with the change of concentration of nanoparticles which is regarded as an important impeding point for heat transfer from rib and the heated surface where heat transfer is increased but the temperature gradient is small due to the fact that the isotherms are circa overlapping at the leading edge of the fin and increases at it develops further from the stagnation point.

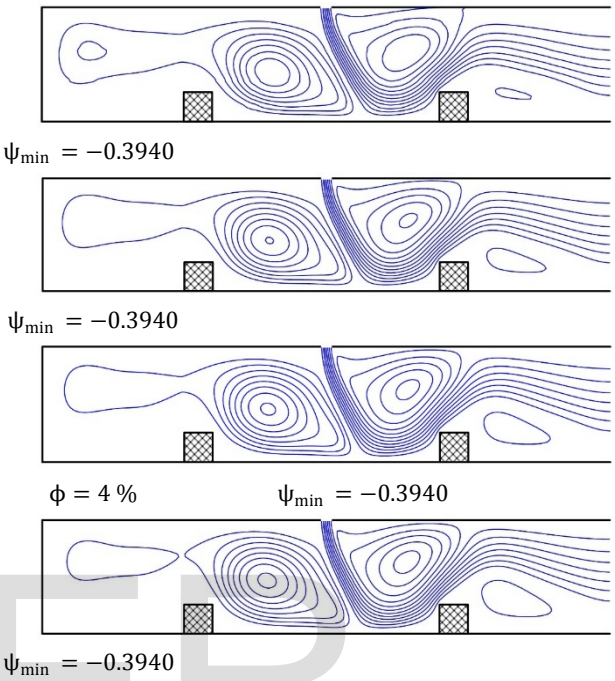


Fig.8. Streamlines For $b/w = 3$ ,$Ri = 0.1$ , $Re = 141$.

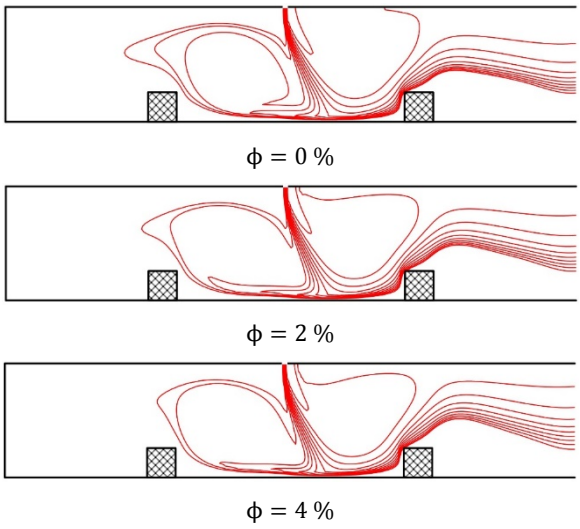

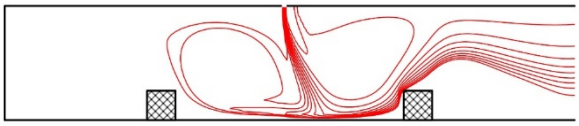

$\phi = 6\ \%$

Fig.9. Isotherms For b/w = 3 ,Ri = 0.1 , Re = 141

### 3.2 Effect of Richardson Number

The effects of Richardson number are studied upon investigation, where the flow and temperature distribution are considered. The increase in Richardson number means an increase in the buoyancy forces and thus the effects of the momentum of initial jet deteriorate as the flow is dominated by buoyancy effects. The streamlines and isotherms are shown in Figures 11 and 12. They are for a case of downward facing jet, where the flow is impeded by the forces of buoyancy which means that with the as the value of Richardson number increment the wall friction, heat transfer and impinging velocity are lessen. It can be seen that when Richardson number increases adequately, negative flow in the wall jet region eventually separates from the surface and is converged again at the leading edge of the fins. As the values of Richardson number progress the jet does not impinge on the surface and the fluid is drawn outward along the surface of the fins. The increase in Richardson number has various effect on the Nusselt number which can be observed in Figures 13,14,15 and compared to the isotherms obtained from Figure 11 and 12, where the average local Nusselt is plotted against the values of Richardson number for four types of concentration of nanoparticles Pure Water (0%) and 2,4,6 % respectively. Near the leading edge of the fins the local stagnant flow causes a poor heat transfer, where a sudden increase in the heat transfer is shown at upstream which is due to the rise in the flow velocity leading to the peak Nusselt number value. A dramatic decrease in Nusselt number is acquired due to the growth of the thermal boundary layer over the upper surface of the fin. Almost before the trailing edge of the fin, the value of Nusselt number increases slowly where the heat transfer area causes an augmented heat transfer. The recirculation effect is increased as the Richardson number is increased which is due to the domination of the buoyancy effect which is why a rapid drop in local Nusselt number can be expected after the fin due to that effect. The effect of large values of Richardson number on average Nusselt number is that a drastic decrease in Nusselt number is linked to the larger values or Richardson number which is due to a dramatic change in the flow field as the buoyancy forced being to dominate the flow begins to retard and the momentum of impingement is affected by those forces which in turn decreases the characteristics of surface transport. Furthermore, it can be found that Nusselt number Increases then decreases for the same b/a keeping Reynolds number constant which means that temperature gradient along rib height is larger for ribs due to higher thermal resistance for a fixed profile area. The change of local Nusselt number along the surface of the rib is shown in Figure 10 for $\mathrm{Re} = 200, \mathrm{Ri} = 0.1, \phi = 4\ \%$.The local Nusselt number for the vertical distance along the rib's side are also included as part of the surface position on the x-axis of the plot. At the left side of the fin near the bottom, due to local stagnant flow a low heat transfer rate is observed. A sudden increase in the local Nusselt number is observed at upstream edge of the rib which is caused by an abrupt increase in the flow velocity which leads to an utmost value of local Nusselt number. A rapid decrease in the heat transfer rate is shown and thus the local Nusselt number drops gradually to the locally to a floor value and remains in that condition till reaching the other end, due to the effect of the thermal boundary growth over the tip surface of the rib. A slight increase in the local Nusselt number is achieved near the rib's right upper corner. This increase is elucidated by the augmentation in heat transfer that is caused by the increase in the heat transfer are around the corner. Farther from the tip of the rib, a rapid decrease in the local Nusselt number is observed at the lower end of the trailing edge which is explained by the recirculation effect of the secondary vortex. It is concluded that for the given aspect ratios as the rib's height is increase a lower Nusselt number is achieved. This is due to the sharp edges experienced by the flow and the reduction in the flow area which leads to a sudden increase in the flow velocity. Conversely, for the case of a/b equal to 1.5 and 2 a higher Nusselt number value is observed due to the reduction in the rib's height. This leads to a decrease in the number of sharp edges that the flow encounter through its path.

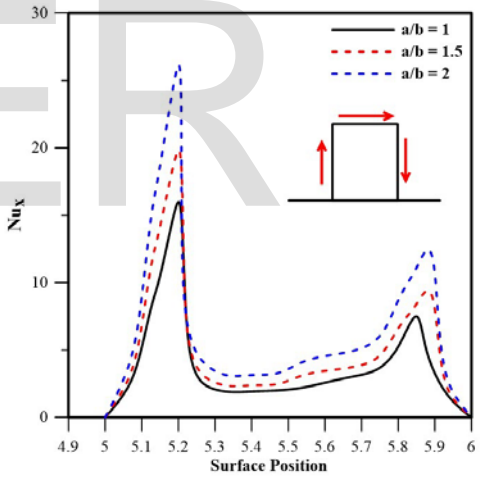


Fig.10. Local Nusselt Numberat rib's surface$\mathrm{Re} = 200, \mathrm{Ri} = 0.1, \phi = 4\%$

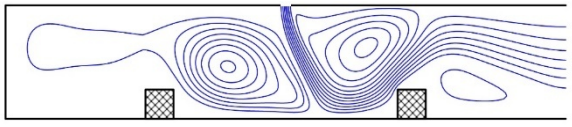

$\psi_{min} = -0.4086$ $\mathrm{Ri} = 0.1$ $\psi_{max} = 0.6157$

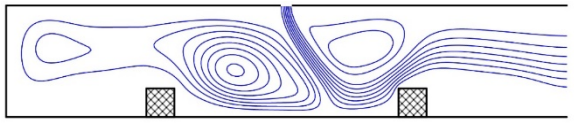

$\psi_{min} = -0.4106$ $\mathrm{Ri} = 0.2$ $\psi_{max} = 0.5456$

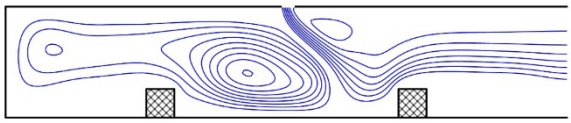

$\psi_{min} = -0.4529$ Ri = 0.4 $\psi_{max} = 0.4708$

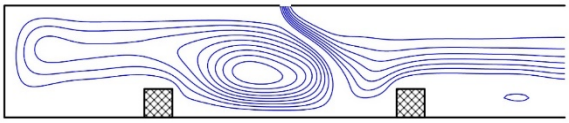

$\psi_{min} = -0.4940$ Ri = 0.6 $\psi_{max} = 0.4484$

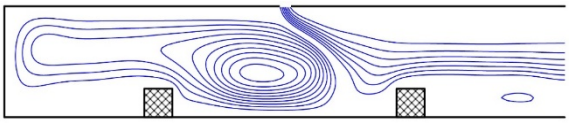

$\psi_{min} = -0.5307$ Ri = 0.8 $\psi_{max} = 0.4524$

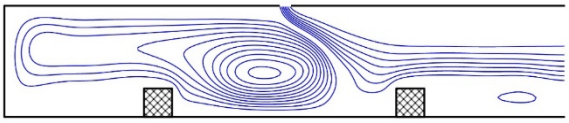

$\psi_{min} = -0.5658$ Ri = 1 $\psi_{max} = 0.4589$

Fig.11. Effect of Richardson Number on Streamlines for $b/w = 3$ $and$ $\phi = 4\ \%$

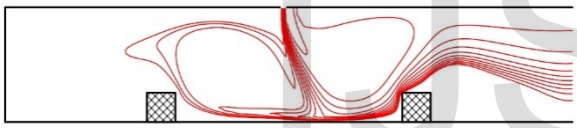

Ri = 0.1

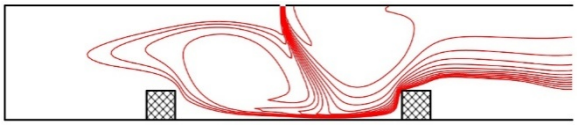

Ri = 0.2

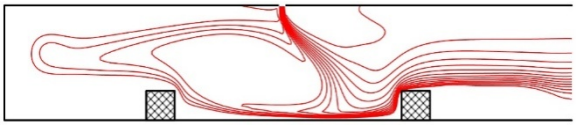

Ri = 0.4

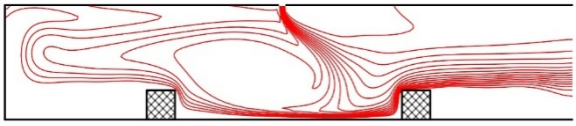

Ri = 0.6

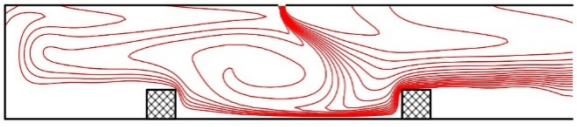

Ri = 0.8

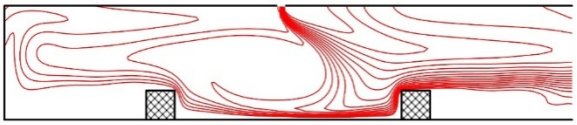

Ri = 1

Fig.12. Effect of Richardson Number on Isotherms for $b/w = 3$ $and$ $\phi = 4\ \%$

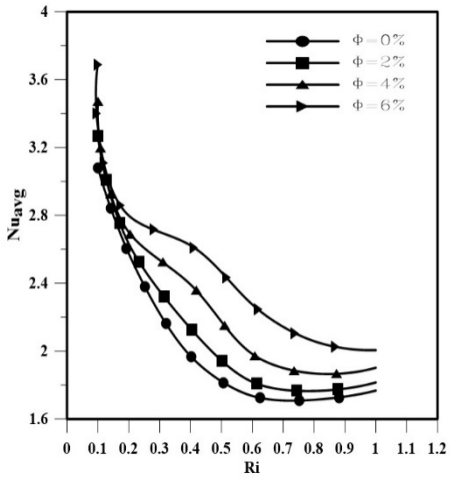


Fig.13. Effect of Richardson Number For b/w = 3

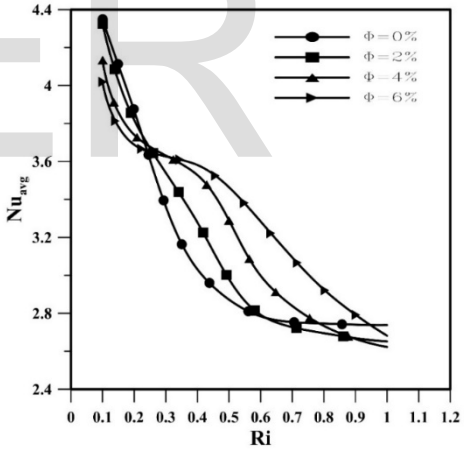


Fig.14. Effect of Richardson Number For b/w = 4

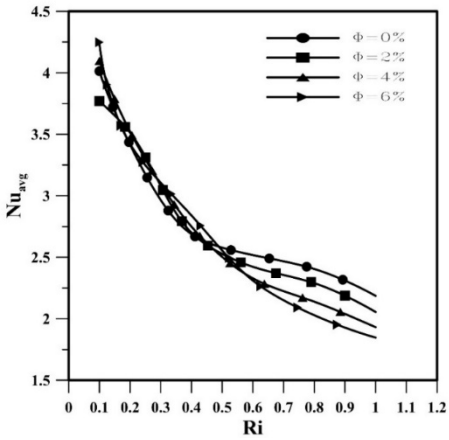


Fig.15. Effect of Richardson Number For $b/w = 5$

### 3.3 Effect of Reynolds Number

The effect of Reynolds number on the streamlines and isotherms is shown in Figures 17 and 18. Although a fully developed flow is indicated at the end of the computational domain, when the value of Reynolds number varies from 50 till 400, for low values of Reynolds number the flow spreads over a larger area unlike higher values of Reynolds number as seen in Figure 16 for each case where this is caused to the shear force of the fluid. The formation of strong eddy downstream from the leading edge of the fin which is due to the flow nature of the wall jet where the vortex is formed at the back end of the fin. The size of the vortex is augmented as the Reynolds number is increased from 50 till 400 where the recirculation moves from the front end of the fin to the left side of the wall as Reynolds number is increased from 50 till 200.When Reynolds number is increased from 200 till 250 a back flow is experienced due to adverse pressure gradient along the wall where the vortex size is miniscule when compared to that when Reynolds number was 50.As Reynolds number is increased from 250 till 400 the backflow experienced in the case of Reynolds number 250 is worst where the velocity difference is dramatically changes and it degrades from the value of Reynolds number is equal to 300 which is observed by the values of the stream function shown. As the thermal boundary layer grows from Reynolds number 50 till 400 a declining value of convection heat transfer coefficient is expected due to the presence of high temperature gradients around the stagnation point region where the local Nusselt number value is very high.

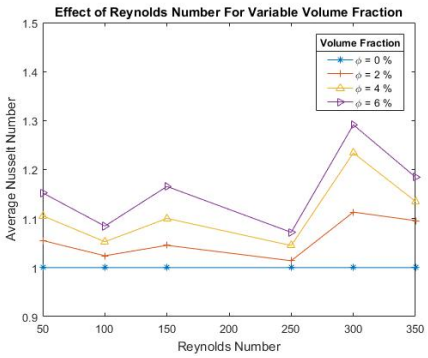


Fig.16. Effect of Reynolds Number for b/w=3, RI=0.1

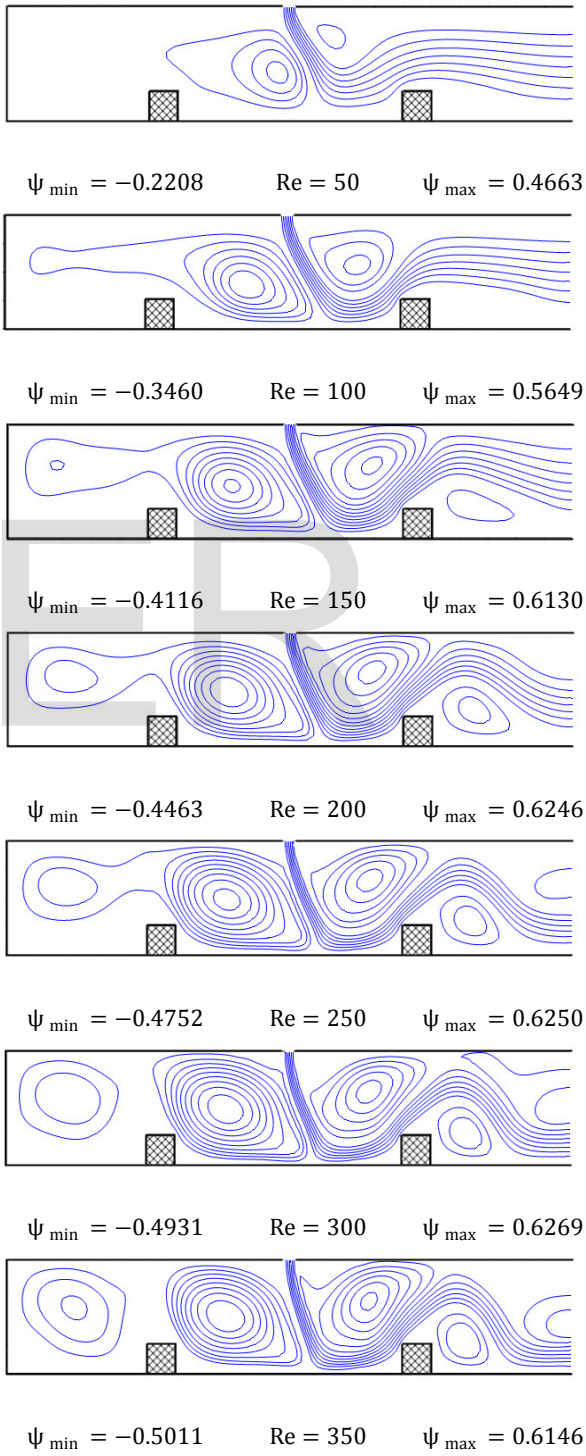

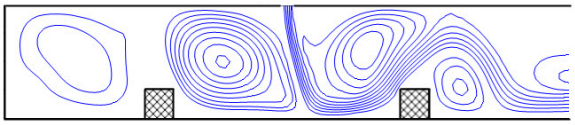

$\psi_{min} = -0.5086$ $\quad Re = 400$ $\quad \psi_{max} = 0.6011$

Fig.17. Streamlines for b/w=3 ,Ri=0.1 and ϕ=2 %

$Re = 400$

Fig.18. Isotherms for b/w=3 ,Ri=0.1 and ϕ=2 %

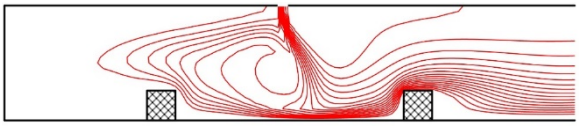

$Re = 50$

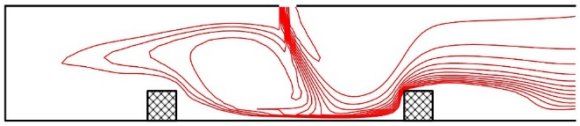

$Re = 100$

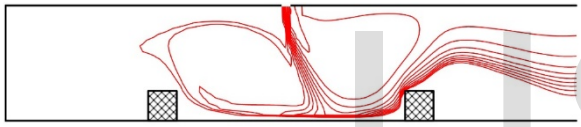

$Re = 150$

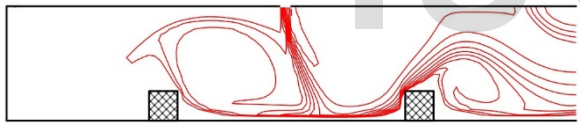

$Re = 200$

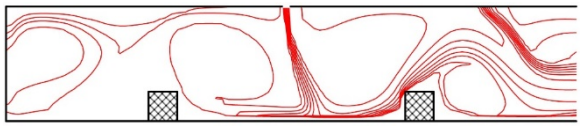

$Re = 250$

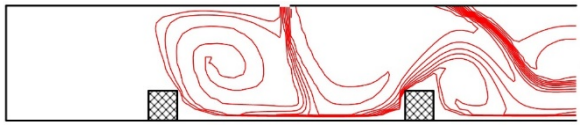

$Re = 300$

$Re = 350$

## 4 Correlations for the Average Nusselt Number

The results from the FORTRAN program for the average Nusselt number over the range of investigated parameter including: Richardson number, solid volume fraction and Reynolds number are fitted for various conditions with a multivariate second order polynomial regression model, which is more applicable than the numerical values.

$$\begin{aligned} Nu = {} & 2.9172Ri^2 - 0.039481Ri\phi + 0.0056\phi^2 \\ & - 4.5688Ri + 0.059053\phi \\ & + 3.4262 \end{aligned} \tag{15}$$

Limitations : $b/w = 3{,}0 <$ Maximum Deviation

$Ri \leq 1{,}0 \leq \phi \leq 0.06$ : 15.23%

$$\begin{aligned} Nu = {} & 1.8581Ri^2 + 0.0554Ri\phi + 0.0039\phi^2 \\ & - 3.8491Ri - 0.0341\phi + 4.5577 \end{aligned} \tag{16}$$

Limitations : $b/w = 4{,}0 <$ Maximum Deviation

$Ri \leq 1{,}0 \leq \phi \leq 0.06$ : 17.75%

$$\begin{aligned} Nu = {} & 2.7172Ri^2 - 0.1206Ri\phi + 0.0042\phi^2 \\ & - 4.7219Ri + 0.0236\phi + 4.3050 \end{aligned} \tag{17}$$

Limitations : $b/w = 5{,}0 <$ Maximum Deviation

$Ri \leq 1{,}0 \leq \phi \leq 0.06$ : 14.90%

## 5 Conclusions

Numerical investigation for laminar mixed convection over flat plate with two ribs using nanofluids were carried out. The governing equations were solved by finite volume method using TDMA utilizing SIMPLE with assumptions and appropriate boundary conditions. The results were predicted based on the average Nusselt number.it can be concluded that:

- Increasing the aspect ratio of the rib depends on Reynolds number and the channel height however when Nusselt Number is decreased when the critical Reynolds number is achieved where vortices are present and decreases the heat transfer rate.
- Increasing the solid volume fraction in-fact increases the Nusselt Number when reviewed with the results using φ=2,4,6%.

- An increase in pressure drop over the ribs is observed when increasing the Reynolds number and increasing the rib's aspect ratio over 2 where vortices and backflow occurs due to excessive adverse pressure gradient along the channel wall.
- The buoyancy effect increases with the increase of Richardson number and hence improving the heat transfer rate. The critical rib aspect ratio becomes larger when increasing Richardson number, however if Richardson number is increased forced convection becomes dominant and the effect of buoyancy diminishes.

## REFERENCES

[1] M. Rebay, S. Kakaç, R.M. Cotta, Microscale and Nanoscale Heat Transfer: Analysis, Design, and Application, CRC Press, 2016.

[2] J.C. Han, S. Dutta, S. Ekkad, Gas Turbine Heat Transfer and Cooling Technology, Second Edition, CRC Press, 2012.

[3] H.-L. Li, H.-W.D. Chiang, C.-N. Hsu, Jet Impingement and Forced Convection Cooling Experimental Study in Rotating Turbine Blades, Int. J. Turbo Jet Engines. 28 (2011). .

[4] W. El-Maghlany, M. Teamah, A.E. Kabeel, A. Hanafy, Premium jet cooling with two ribs over flat plate utilizing nanofluid mixed convection, Therm. Sci. (2015) 56–56.

[5] M.A. Teamah, M.M. Khairat Dawood, A. Shehata, Numerical and experimental investigation of flow structure and behavior of nanofluids flow impingement on horizontal flat plate, Exp. Therm. Fluid Sci. 74 (2016) 235–246.

[6] O. Manca, D. Ricci, S. Nardini, G. Di Lorenzo, Thermal and fluid dynamic behaviors of confined laminar impinging slot jets with nanofluids, Int. Commun. Heat Mass Transf. 70 (2016) 15–26.

[7] A. Heshmati, H.A. Mohammed, A.N. Darus, Mixed convection heat transfer of nanofluids over backward facing step having a slotted baffle, Appl. Math. Comput. 240 (2014) 368–386.

[8] R. Dutta, A. Dewan, B. Srinivasan, CFD study of slot jet impingement heat transfer with nanofluids, Proc. Inst. Mech. Eng. Part C J. Mech. Eng. Sci. 230 (2016) 206–220. .

[9] C.T. Nguyen, F. Desgranges, N. Galanis, G. Roy, T. Maré, S. Boucher, H. Angue Mintsa, Viscosity data for Al2O3–water nanofluid—hysteresis: is heat transfer enhancement using nanofluids reliable?, Int. J. Therm. Sci. 47 (2008) 103–111.

[10] J.-B. Huang, Numerical Study of a Confined Axisymmetric Jet Impingement Heat Transfer with Nanofluids, Engineering. 05 (2013) 69–74.

[11] M.K. Singh, D. Yadav, S. Arpit, S. Mitra, S.K. Saha, Effect of nanofluid concentration and composition on laminar jet impinged cooling of heated steel plate, Appl. Therm. Eng. 100 (2016) 237–246.

[12] S.E.B. Maïga, S.J. Palm, C.T. Nguyen, G. Roy, N. Galanis, Heat transfer enhancement by using nanofluids in forced convection flows, Int. J. Heat Fluid Flow. 26 (2005) 530–546.

[13] I. Dagtekin, H.F. Oztop, Heat transfer due to double laminar slot jets impingement onto an isothermal wall within one side closed long duct, Int. Commun. Heat Mass Transf. 35 (2008) 65–75.

[14] R.S. Vajjha, D.K. Das, Experimental determination of thermal conductivity of three nanofluids and development of new correlations, Int. J. Heat Mass Transf. 52 (2009) 4675–4682.

[15] K.S. Hwang, J.H. Lee, S.P. Jang, Buoyancy-driven heat transfer of water-based Al2O3 nanofluids in a rectangular cavity, Int. J. Heat Mass Transf. 50 (2007) 4003–4010.

[16] J.C. Maxwell, A Treatise on Electricity and Magnetism, Clarendon Press, 1873.

[17] A. Einstein, A New Determination of Molecular Dimensions, Ann. Phys. 324 (1906) 289–306.

[18] H.A. Mohammed, A.N. Al-Shamani, J.M. Sheriff, Thermal and hydraulic characteristics of turbulent nanofluids flow in a rib–groove channel, Int. Commun. Heat Mass Transf. 39 (2012) 1584–1594.

[19] O. Manca, P. Mesolella, S. Nardini, D. Ricci, Numerical study of a confined slot impinging jet with nanofluids, Nanoscale Res. Lett. 6 (2011) 188.

[20] S. Patankar, Numerical Heat Transfer and Fluid Flow, Taylor & Francis, 1980.

## NOMENCLATURE

| | |
|---|---|
| A | Area ($m^2$) |
| $Al_2O_3$ | Aluminium-Oxide |
| Ag | Silver |
| a | Rib's Width (m) |
| b | Rib's Height (m) |
| $C_p$ | Specific Heat at Constant Pressure (J/kg. K) |
| CuO | Copper Oxide |
| Cu | Copper |
| D | Rib's Spacing (m) |
| Gr | Grashof Number |
| H | Plate Height (m) |
| h | average heat transfer coefficient ($W/m^2.K$) |
| k | Thermal Conductivity (W/m. K) |
| L | Plate Length (m) |
| Nu | Nusselt number |
| Pr | Prandtl Number |
| q | heat flux ($W/m^2$) |
| Re | Reynolds Number |
| Ri | Richardson Number |
| $SiO_2$ | Silicon dioxide |
| $TiO_2$ | Titanium dioxide |
| T | Temperature (K) |
| u, v | Velocity Components in x, y Direction Respectively (m/s) |
| U, V | Dimensionless Velocity Components in X, Y Direction |
| V | Velocity (m/s) |
| W | Slot Jet Width (m) |
| x, y, z | Cartesian Coordinates |
| X, Y, Z | Dimensionless Cartesian Coordinates |

Greek Symbols

| | |
|---|---|
| $\rho$ | Density ($kg/m^3$) |
| $\phi$ | Solid Volume Fraction |
| $\beta$ | Thermal Expansion Coefficient ($K^{-1}$) |
| $\mu$ | Dynamic Viscosity ($N.s/m^2$) |
| $\nu$ | Kinematic Viscosity ($m^2/s$) |
| $\theta$ | Dimensionless Temperature |
| $\alpha$ | Thermal Diffusivity ($m^2/s$) |

Subscripts

| | |
|---|---|
| s | Surface |
| j | jet |
| nf | nanofluid |
| eff | effective |
| bf | base fluid |
| p | particle |

Abbreviations

| | |
|---|---|
| FVM | Finite Volume Method |
| SIMPLE | Semi-Implicit Method for Pressure Linked Equations |
| TDMA | Tri-Diagonal Matrix Algorithm |